Surface Science 605 (2011) 1999-2005

Mapping the local reaction kinetics by PEEM: CO oxidation on individual (100)-type grains of Pt foil

D. Vogel[a,b], C. Spiel[a], Y. Suchorski[a*], A. Urich[c], R. Schlögl[b], G. Rupprechter[a]

[a]Institute of Materials Chemistry, Vienna University of Technology, Getreidemarkt 9, 1060 Vienna, Austria
[b]Fritz-Haber-Institut der Max-Planck-Gesellschaft, Faradayweg 4-6, 14195 Berlin, Germany
[c]Photonics Institute, Vienna University of Technology, Gußhausstr. 27-29, 1040 Vienna, Austria

[*] Corresponding author: e-mail yuri.suchorski@imc.tuwien.ac.at,

Received 06 May 2011; Accepted 25 July 2011; Available online 02 August 2011

Abstract

The locally-resolved reaction kinetics of CO oxidation on individual (100)-type grains of a polycrystalline Pt foil was monitored *in situ* using photoemission electron microscopy (PEEM). Reaction-induced surface morphology changes were studied by optical differential interference contrast microscopy and atomic force microscopy (AFM). Regions of high catalytic activity, low activity and bistability in a (p,T)-parameter space were determined, allowing to establish a local kinetic phase diagram for CO oxidation on (100) facets of Pt foil. PEEM observations of the reaction front propagation on Pt(100) domains reveal a high degree of propagation anisotropy both for oxygen and CO fronts on the apparently isotropic Pt(100) surface. The anisotropy vanishes for oxygen fronts at temperatures above 465 K, but is maintained for CO fronts at all temperatures studied, in the range of 417 to 513 K. A change in the front propagation mechanism is proposed to explain the observed effects.

Keywords: Surface reactions; Photoemission electron microscopy; Atomic force microscopy; Platinum; CO oxidation

1. Introduction

Although catalytic CO oxidation on Pt group metals is one of the most extensively studied surface reactions in heterogeneous (model) catalysis [1], the detailed comparison of the catalytic behaviour of differently-oriented surfaces is still difficult. The problems are mainly related to limitations of creating exactly the same experimental conditions for different samples, since even small variations of temperature or pressure near the transition points may induce kinetic transitions from a catalytically active to an inactive state or vice versa [2]. A practicable approach in surface physics, when e.g. adsorption or diffusion are studied in parallel on differently-oriented facets on the same field emitter tip [3], fails in the case of surface reactions due to noise-induced transitions on the small (nm) size facets [4] (i.e. rapid adsorbate diffusion "wipes out" structural differences). However, the individual differently-oriented grains of polycrystalline foils seem to be suitable objects for such studies, due to their mesoscopic (μm) size. A macroscopic sample of about 10x10 mm^2 contains many μm-sized differently-oriented facets which are exposed to exactly the same conditions during catalytic experiments, either in UHV or at high-pressure conditions. The problem of the evaluation of the local catalytic properties of individual grains can then be solved, at least for CO oxidation, using photoemission electron microscopy (PEEM) as a method for local kinetic measurements, as already shown in our preceeding study [5]. The idea to apply PEEM for such studies is based on the correlation of the PEEM intensity with catalytic activity, as observed earlier in averaging studies on Pt single crystal surfaces [6]. Translated to the local studies on individual grains of a polycrystalline Pt-foil, this idea allowed to pursue the kinetic transitions during the reaction and even to create local kinetic phase diagrams for individual crystalline grains [5], as is described in detail below.

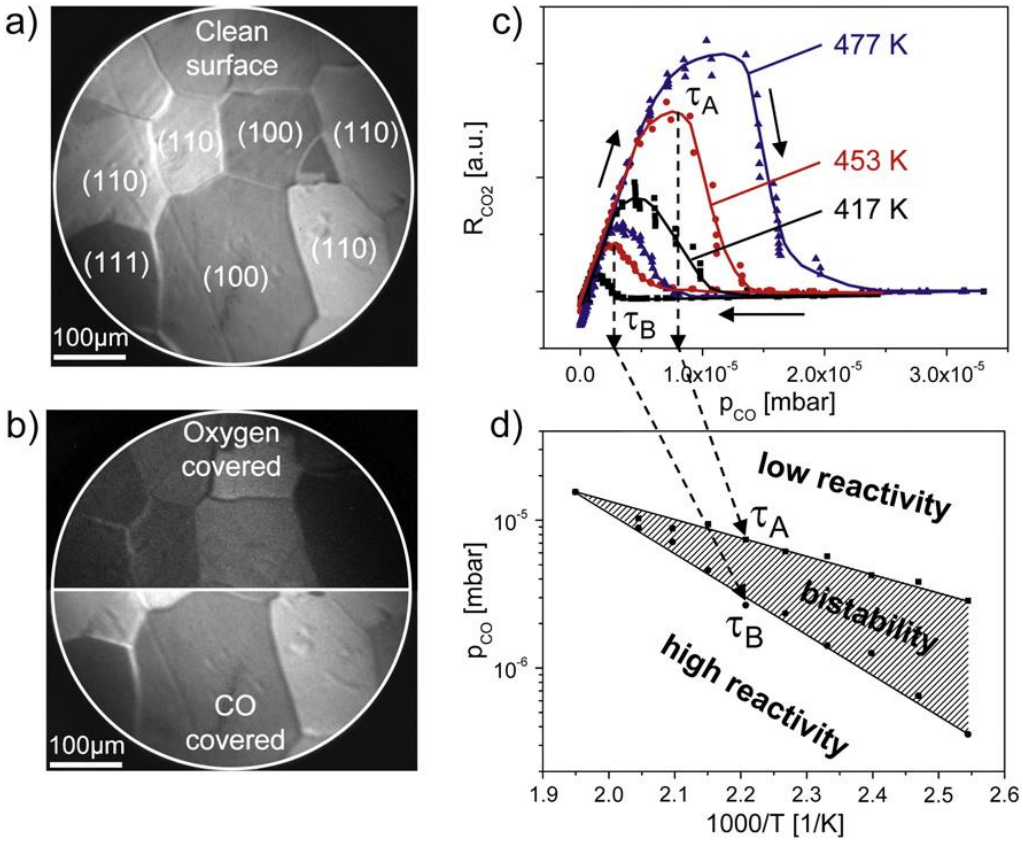

Fig. 1. Global kinetics of CO oxidation on Pt foil.
(a) PEEM image of the clean Pt foil. The surface termination of the individual grains is indicated.
(b) PEEM images of the oxygen-covered (top) and the CO-covered (bottom) Pt foil. The oxygen-covered surface appears dark in PEEM since adsorbed oxygen increases the work function of the Pt surface.
(c) Hysteresis in the global CO_2 production rate at cyclic variation of the CO pressure at constant O_2 pressure of 1.3×10^{-5} mbar and at temperatures of 417 K (black squares), 453 K (red dots) and 477 K (blue triangles). The τ_A and τ_B values deduced from the hysteresis curves were used for the kinetic phase diagram in Fig. 1d.
(d) Global kinetic phase diagram of CO oxidation on polycrystalline Pt foil, obtained by mass spectroscopy.

In the current contribution we concentrate on an individual [100]-oriented grain of a Pt foil since CO oxidation on Pt(100) single crystal surfaces has already been studied intensively: temporal oscillations in the CO_2 reaction rate were observed and could be correlated to work function oscillations [7] and to periodic variations of the LEED pattern corresponding to (hex) and (1x1) reconstructions [8-12]. In early attempts, the existence range of oscillations was evaluated by a p_{CO}-p_{O2}-diagram at fixed temperature [13], a predecessor of the currently-used kinetic phase diagrams in which catalytic properties of a reaction system can be summarized over a wide range of external parameters such as temperature and partial pressures of reactants [14-16]. Scanning photoemission microscopy was first applied to monitor the Pt(100) surface during the CO oxidation reaction [17,18], but a *real time* imaging of the spatio-temporal patterns formed during the reaction was only possible after the development of photoemission electron microscopy (PEEM), due to its parallel imaging principle [1,19]. In a first systematic PEEM study of the CO oxidation reaction on a Pt(100) single crystal in the oscillatory regime the kinetic oscillations of the CO_2 production rate could be clearly correlated to the spatio-temporal pattern formation [20]. The propagation of reaction-diffusion fronts on Pt(100) was investigated in more detail using LEEM and selected-area LEED [21-24]. In further PEEM studies, the formation of subsurface oxygen species could be observed at the boundary of oxygen and CO-covered regions [25] and a mechanism for the formation of this oxygen species could be established [26].

Despite the large number of studies performed on Pt(100) single crystal surfaces, most of these studies are restricted to the parameter range of kinetic oscillations, while little attention was paid to the bistability regime. In the present study, we concentrate on the kinetic transitions from the active to the inactive state of the system and vice versa, as well as on the bistable state in between. Since the studied Pt(100) surface is a domain of a polycrystalline foil, we are able to investigate the effect of grain boundaries on the local kinetics. Although polycrystalline foils are suitable model systems for such studies, such foils have yet been investigated by combined microscopic and kinetic

methods very rarely and only under the aspect of kinetic oscillations, and in a rather qualitative way [27,28].

Another focus of the present study is the morphology of the individual (100) grains of the Pt foil and its changes induced by the CO oxidation reaction. In several previous studies some characteristic morphological structures have already been reported. Lauterbach et al. have observed "a pronounced texture with parallel furrows" on the (100)-type grains of a polycrystalline platinum foil by SEM, the size of the furrows ranging from 200 nm up to several µm [27]. In a LEEM study on a Pt(100) single crystal a characteristic step and terrace structure with a mean terrace width of approximately 700 nm to 1 µm is reported [23]. Other authors have shown that the CO oxidation reaction can induce a strong roughening of the platinum surface up to a length scale of 0.1-1 µm [29,30]. Nevertheless, the formation of these features is still not entirely understood. Using PEEM and AFM in the present study we present a model that may explain the mechanism under which these characteristic features (up to the µm range) are developed.

2. Experimental

The experiments were performed in a multifunctional UHV chamber with a base pressure below 10^{-9} mbar. The chamber is equipped with a PEEM (STAIB instruments), a quadrupole mass spectrometer (MKS instruments), sample preparation facilities for sputtering and annealing, and a gas supply system with high-purity reactive gases (O_2: 99.999 %, CO: 99.97 %). The sample consisted of a 10x10 mm^2 polycrystalline Pt foil (MaTecK, 99.99%) flame annealed in air prior to mounting. Furthermore, the sample was cleaned in UHV by repeated cycles of Ar^+ ion sputtering at 1 keV energy and annealing up to 1073 K. The temperature was measured by a NiCr/Ni thermocouple spot-welded to the back of the sample.

The PEEM-image is created by photoelectrons emitted from the sample surface which is irradiated by a UV deuterium discharge lamp (D200, Heraeus) with a cut-off photon energy of 6.8 eV. The intensity of the emitted photoelectrons depends strongly on the local sample work function. This allows to identify the surface termination of individual grains on the Pt foil by selected-area intensity analysis, as described in more detail elsewhere [5,31]. In turn, the local work function varies strongly with the local adsorbate coverage, so it is possible to follow the CO oxidation reaction in situ on *individual* grains of the Pt foil. By analyzing the local PEEM intensities during the reaction also local kinetic information can be obtained, as we have shown recently [5,31]. The local PEEM data can be correlated with the global CO_2 reaction rate measured simultaneously by the mass spectrometer placed in vicinity of the sample.

The surface topography of the (100) domains on the Pt foil was studied with a commercial AFM (NanoMan VS, Veeco) at ambient conditions in tapping mode. A PPP-NCHR probe (Nanosensors) with a nominal tip radius below 10 nm was used. An optical microscope was coupled with the AFM for a preselection of a region of interest from which AFM images were taken. AFM image analysis including linear height profiles was carried out using the Gwyddion Software. In addition, differential interference contrast microscopy (Polyvar 2 MET from Reichert Microscope Services, NA=0.95) was utilized to obtain optical micrographs with enhanced contrast of the Pt foil.

3. Results and discussion

3.1. Global and local reaction kinetics

To compare the local kinetics of CO oxidation on an individual grain on the polycrystalline Pt foil with the averaged (global) kinetics of the whole foil, global MS studies were performed first. The results of such MS studies in the bistability range of CO oxidation are summarized in Fig. 1, where Figs. 1a, b show PEEM images of the clean and adsorbate covered sample, respectively, and Figs. 1c, d the CO_2 production rate and the kinetic phase diagram, respectively. The surface orientation of the grains was determined by comparison of the local PEEM intensity with single crystal work function data (see Ref. [5] and supporting information). As typical for CO oxidation on Pt, the surface is in a high reactivity steady state (predominantly oxygen-covered, Fig. 1b) at low CO pressures with the CO_2 production rate increasing with increasing CO partial pressure (at constant oxygen partial pressure and constant temperature; Fig. 1c). At a certain CO to oxygen pressure ratio CO adsorption prevails over oxygen adsorption, thus drastically reducing the CO_2 production. Adsorbed CO inhibits the dissociative adsorption of oxygen and a kinetic transition to the low reactivity steady state occurs [2]. This transition point in the parameter space is termed transition point τ_A whereas the point of the reverse transition is called τ_B (Fig. 1c). Due to the effective blocking of adsorption sites for oxygen by CO the reverse transition from the inactive to the active state takes place at a lower CO partial pressure τ_B than the transition τ_A. This leads to the hysteresis in the CO_2 production rate as shown in Fig. 1c for three temperatures. Higher temperatures lead to a shift of the hysteresis curves: higher CO partial pressures are required for the kinetic transition and the CO_2 reaction rate is higher. This behaviour can be summarized in a plot called "kinetic phase diagram", based on the analogy to phase transitions in equilibrium thermodynamics [32,33] (in Fig. 1d for the temperature range 393 to 513 K). Such diagrams are a useful representation of the kinetic behaviour of the reaction system, i.e. of the regions of high/low reactivity, bistability and oscillations, and may also effectively illustrate the role of reaction promoters (altering the adsorption/desorption kinetics, sticking etc.) [15,16].

Because the Pt foil consists of crystallites exposing different surface orientation (cf. Fig. 1a), it is expected that

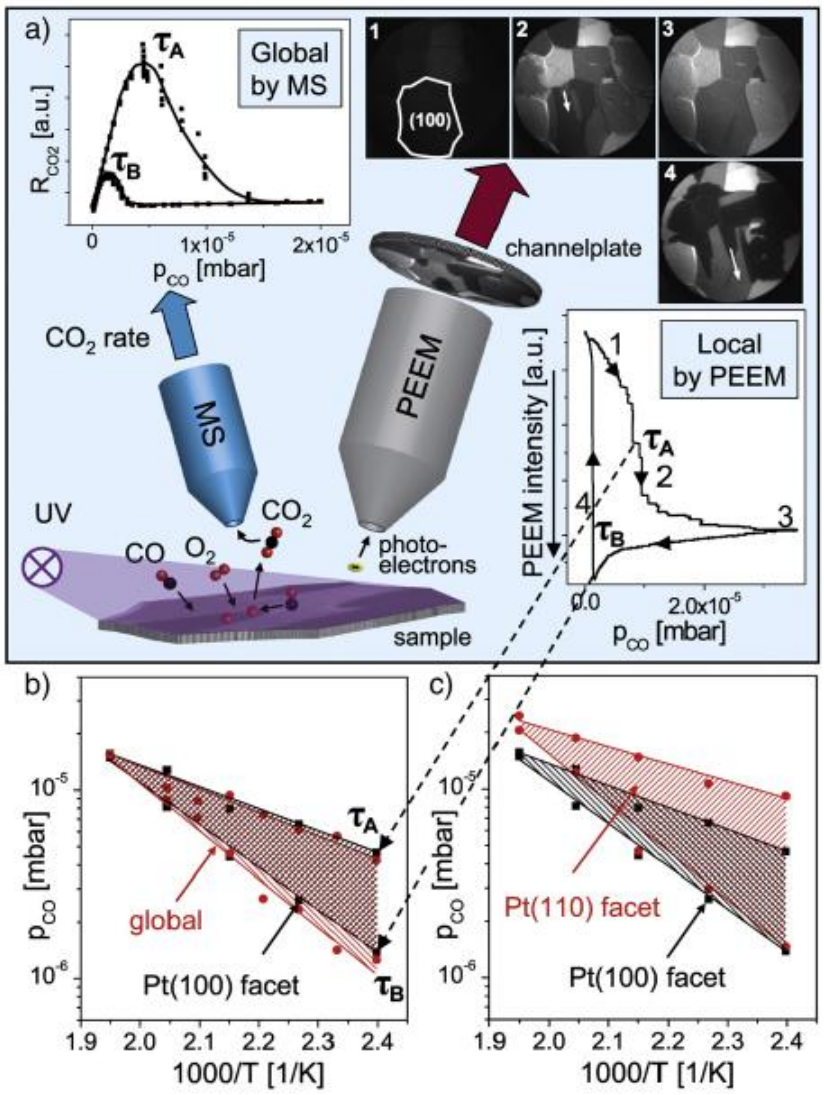

Fig. 2. Local kinetics of CO oxidation on individual crystalline grains of a Pt foil.
(a) Principle of the local kinetic measurements by PEEM. Left inset: Global CO_2 production rate versus CO partial pressure as measured by MS during catalytic CO oxidation at T = 417 K and $p_{O2} = 1.3x10^{-5}$ mbar. Right inset: Hysteresis plot of the local PEEM intensity of an individual Pt(100) facet versus CO partial pressure, as measured *in situ* by PEEM at the same reaction conditions. The selected domain is indicated in frame (1). The numbers along the hysteresis curve indicate the corresponding PEEM frames.
(b) Corresponding kinetic phase diagram for a Pt(100) facet (black squares) in comparison to the global (MS-measured) diagram (red dots).
(c) The same as in (b), but in comparison to a local diagram for a Pt(110) facet (red dots).

the *local* reaction kinetics are different. Thus, we utilize PEEM to determine the local kinetic transitions on individual grains, by evaluation of the local PEEM intensity recorded during real time imaging of the CO oxidation reaction. The principle is illustrated in Fig. 2a: In parallel to the measurement of the global CO_2 production rate by MS, we monitor the local PEEM intensity of a defined area, typically an individual grain of the Pt foil (a [100]-oriented facet = "region of interest" is depicted in inset (1)), during cyclic variation of the CO partial pressure at a constant temperature and constant oxygen partial pressure. The video-frames 1-4 represent characteristic points in the hysteresis cycle and the inset below the frames presents the corresponding local PEEM intensity curve for the (100) grain. The drops/jumps in the local PEEM intensity reflect the local kinetic transitions characteristic for this particular crystalline Pt grain. In frame (1) the surface is oxygen-covered (high-reactivity steady state), frame (2) reflects the transition τ_A. Bright CO fronts are propagating across the (100) facet, resulting in a sharp increase of the intensity that corresponds to a drop in the simultaneously measured CO_2 production rate (note that the PEEM intensity axis has an opposite direction to the MS axis in Fig. 1c). Frame (3) corresponds to a CO covered surface (low-reactivity steady state) and frame (4), in turn, shows a sharp decrease of the intensity at the transition point τ_B when the surface

switches back to an oxygen-covered state. Note the propagating dark oxygen fronts in this frame. The transition points τ_A and τ_B obtained from series of such measurements at different temperatures result in the local kinetic phase diagram shown in Fig. 2b, which is displayed together with the global diagram of Fig. 1d. At first glance, the differences between the global and the local diagram seem rather insignificant, thus questioning this approach. However, the similarity can be rationalized considering that the polycrystalline Pt-foil consists to almost 50% of [100]-oriented grains [27] (this statistics is not necessarily reflected by one PEEM image since only a small part of the Pt foil is imaged), and thus it is reasonable that the averaged MS diagram differs not much from the local Pt(100) diagram. Nevertheless, comparison of the local diagrams measured for the specific Pt(100) facet and for the neighbouring Pt(110) grain (cf. Fig. 1a) shows significant differences, as evident from Fig. 2c. The clear differences between the local diagrams for [110]- and [100]-oriented facets indicate a rather independent catalytic behaviour of individual crystalline grains of mesoscopic size with respect to the CO oxidation reaction. The main advantage of the present PEEM-based kinetic measurements, i.e. to create identical experimental conditions for different crystallographic orientations and to obtain corresponding data for the different orientations *in one experiment*, is thus crucial for studies of this reaction system.

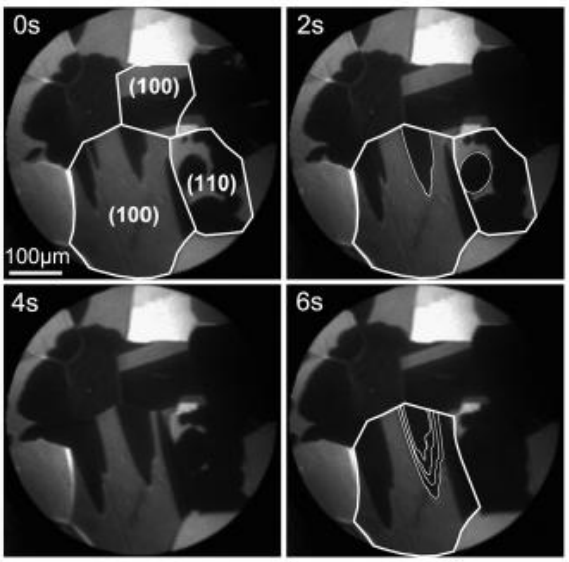

Fig. 3. Propagation of reaction fronts (here oxygen fronts) on polycrystalline Pt foil during catalytic CO oxidation at T = 417 K and p_{O2} = 1.3x10^{-5} mbar (image frames recorded at an interval of 2s). Regions of interest (two Pt(100) domains in comparison with a Pt(110) domain) are marked in the frame "0s". Note the different shape of the propagating fronts on the (100) and (110) domains as marked in the frame "2s". In the frame taken at 6s, the front positions at 0s, 2s, 4s and 6s are outlined in white.

3.2. Surface morphology and reaction fronts

In the following we focus on the propagation of reaction-diffusion fronts on specific Pt(100) grains and its correlation to the surface morphology. Figure 3 shows a series of PEEM image frames recorded during a CO pressure sweep at 417 K and constant p_{O2} = 1.3x10^{-5} mbar, illustrating the transition from the CO-covered (inactive) to the oxygen-covered (active) state. The dark regions represent the propagating oxygen fronts whereas the brighter regions are still CO-covered. The fronts exhibit a pronounced anisotropy, although both possible phases of the (100) surface are expected to be isotropic (i.e. the quasi-hexagonal structure of the clean surface, typically referred to as the (hex) phase [34], and the unreconstructed (1x1) phase formed upon CO or oxygen adsorption [9,10,35]). STM observations, however, have revealed a strong surface roughening during the adsorbate-induced surface transition from the (hex) to the (1x1) phase upon which entire rows of Pt atoms are collectively ejected and form elongated ad-islands [36]. This can be explained by the required compensation of the difference in the surface atom density: the (hex) phase is ~20% more densely packed than the (1x1) phase [37] (see also corresponding ball models in Fig. 7). The size of the "ejected islands" depends on temperature and varies between ~15 Å at 300 K [36] and 70 Å at 460 K [38]. Therefore, even in the "ideal" case neither of the surface configurations can be considered as isotropic. Nevertheless, at first glance the observed high degree of the front anisotropy is astonishing, particularly when compared to that on the neighboring (110) grain (visible e.g. in frames 1 to 3 of Fig. 3). On (110), elliptical fronts are formed due to the known atomic scale anisotropy of the (110) substrate, with a ratio of ~2 for the front velocities along the [1$\bar{1}$0] and [001] directions [31], well in agreement with single crystal data [39].

To understand the striking degree of the front anisotropy on (100) domains, we have investigated the surface morphology of the two neighboring [100]-oriented grains highlighted in PEEM frame 1 of Fig. 3. The surface morphology was examined in more detail by using optical differential interference contrast microscopy and AFM and our observations were compared to earlier STM reports by Borg et al. [36].

Figures 4a, b show PEEM frames of the clean Pt surface (a) and of the Pt surface with propagating oxygen fronts on the two neighboring (100) domains, with the propagation directions significantly differing from each other (b). In turn, the optical micrograph (Fig. 4c) taken after many reaction cycles clearly shows a hill-and-valley surface morphology, which coincides with the front propagation directions. Figures 4d and 4e display corresponding AFM micrographs of the two neighboring grains revealing ca. 20 nm deep and 400-600 nm wide grooves aligned along the propagation directions. Surface structures of similar size have been previously reported in the context of catalytic CO oxidation on Pt surfaces: using scanning electron microscopy Lauterbach et al. have observed parallel furrows (size range of 200 nm up to several µm) on (100)-

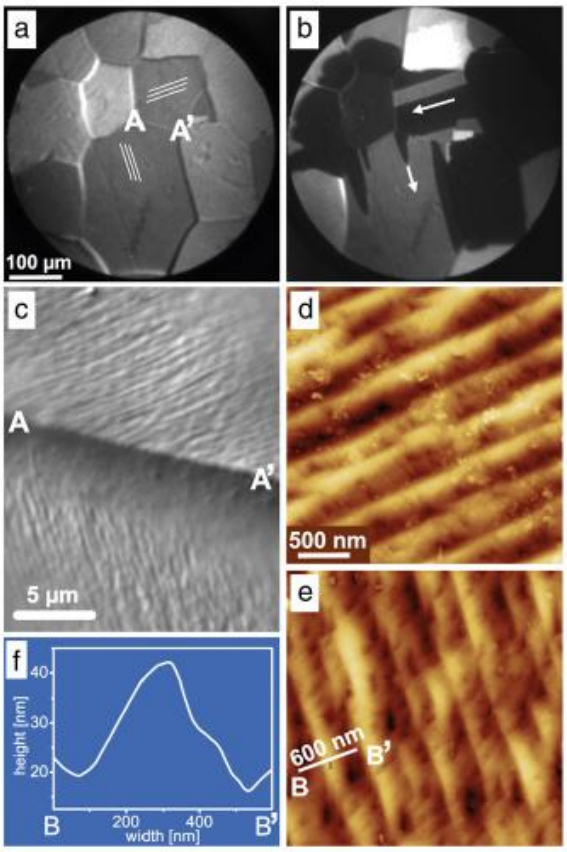

Fig. 4. (a) Clean Pt foil imaged by PEEM. The AA' line denotes the grain boundary between two (100) domains. (b) Snap-shot during the transition τ_B: anisotropic propagation directions of the reaction fronts on the neighboring (100) domains differ from each other. (c) Optical micrograph of the grain boundary region AA'. (d) and (e) AFM images of the neighboring (100) domains. (f) Line scan across the BB' line in (e). The grooves imaged in (c)-(e) are schematically indicated in (a). The reaction front propagation directions (b) coincide with the directions of the grooves in (c) and are indicated in (a).

type grains of a polycrystalline Pt foil, the direction of which correlated with the propagating reaction fronts [27]. Swiech et al. observed a step and terrace structure on a Pt(100) single crystal surface with a mean terrace width of approximately 700 nm [23], which was assigned to a miscut of their single crystal.

The formation of such grooves on (100)-type grains can be explained in the following way: As already mentioned, the adsorbate-induced surface phase transition from the (hex) to the (1x1) phase is accompanied by the formation of elongated (ad-)islands [36,37]. Upon removing the adsorbate a reverse transition takes place, when the less densely packed (1x1) phase covered with ~20% of ad-islands has to transform back into the close-packed (hex) reconstruction. This may proceed not simply through a direct absorption of the adatoms into the (sub)surface layer, which would require quite extensive mass transport, but may proceed via creation of subsurface vacancies, which can coalesce by diffusion to steps and additionally increase the total surface roughness [40]. The CO oxidation reaction additionally enhances the roughening of the surface, since the reaction front propagation involves the surface phase transition, so one can conclude that after numerous repeats of the adsorbate-induced surface phase transition, mesoscopic grooves on the order of several hundred nm width and around 20 nm height are created. Once the grooves are formed, they may have, in turn, an influence on the direction of the reaction front propagation.

To learn more about the propagation of the reaction-diffusion fronts, the role of the reaction temperature was also studied. Figure 5 shows the behaviour of propagating CO fronts during the transition from the active (dark) to the inactive (bright) state at constant oxygen pressure p_{O2} = $1.3x10^{-5}$ mbar, at two different temperatures of 417 K and 513 K. The PEEM images in Fig. 5a, b reveal that at both temperatures the CO fronts are highly anisotropic and oriented along the grooves of the (100) domain. For the whole temperature range, bright fringes are observed separating the CO- and oxygen-covered regions, which are illustrated by intensity line scans (Fig. 5c, d).

Figure 5e shows the temperature dependence of the CO front velocities, which is strong along the grooves (black squares) and basically negligible across the grooves (red dots). The values which are in the low µm/s range are in qualitative agreement with literature data on Pt(100) single crystals [20]. We apply Luther's equation $v(T) \approx a\sqrt{k(T) \cdot D(T)}$ describing the temperature dependence of the propagation velocity *v(T)* of a reaction-diffusion front [41]. *D(T)* is the CO diffusion coefficient and *k(T)* is the effective first-order reaction rate constant of the reaction. The corresponding fit to the front propagation along the grooves obtained with the *D(T)* and *k(T)* values from single crystal studies [13] is in good agreement with our experimental data. This indicates that the reaction fronts along the "faster direction" on the individual (100) domains of the polycrystalline foil behave very similar as on the corresponding Pt(100) single crystal. The velocity along the "slower direction" can hardly be fitted with the literature data of the Pt(100) single crystal, since the surface structure profile in this direction can be rather compared to a stepped (100) surface (see discussion below), for which the surface diffusion is different from the "flat" Pt(100) [42]. Therefore, the fitting parameters were set free and a value of 11.3 kcal/mol for the effective activation energy was obtained from the red line in Fig. 5e.

The mechanism of CO front propagation was proposed already in 1994 (for the oscillating CO oxidation) [20]: on the oxygen covered surface, CO adsorbs at some defects (in the present case at the domain boundaries) and CO_2 is formed, leaving behind a region where the adsorbate coverage is low enough to initiate the (1x1) → (hex) surface phase transition. Since the sticking coefficient for oxygen is lowered to approximately 10^{-3}-10^{-4} on the (hex) phase from ~0.1 on the (1x1) phase [11], oxygen is unlikely to adsorb in this region and the CO molecules can diffuse

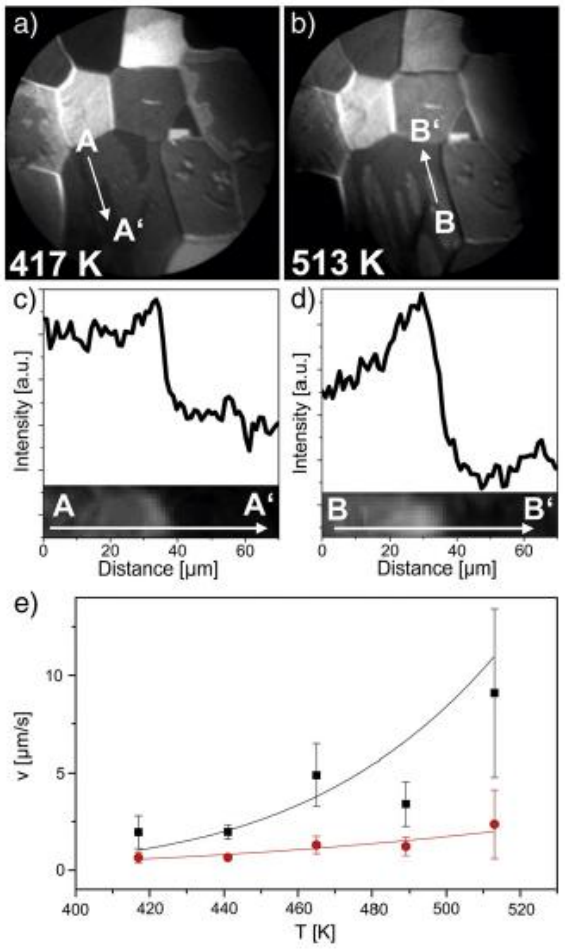

Fig. 5. Temperature dependence of the CO front propagation. (a) and (b) PEEM images of the CO fronts recorded during the transition τ_A at $p_{O2} = 1.3x10^{-5}$ mbar, at 417 K and 513 K, respectively.(c) and (d) Intensity line scans across the CO front along AA' and BB'.(e) Temperature dependence of the front propagation velocities along (black squares) and across (red dots) the grooves on the (100) domain (see Fig. 4). The solid lines are fits using Luther's equation (see text).

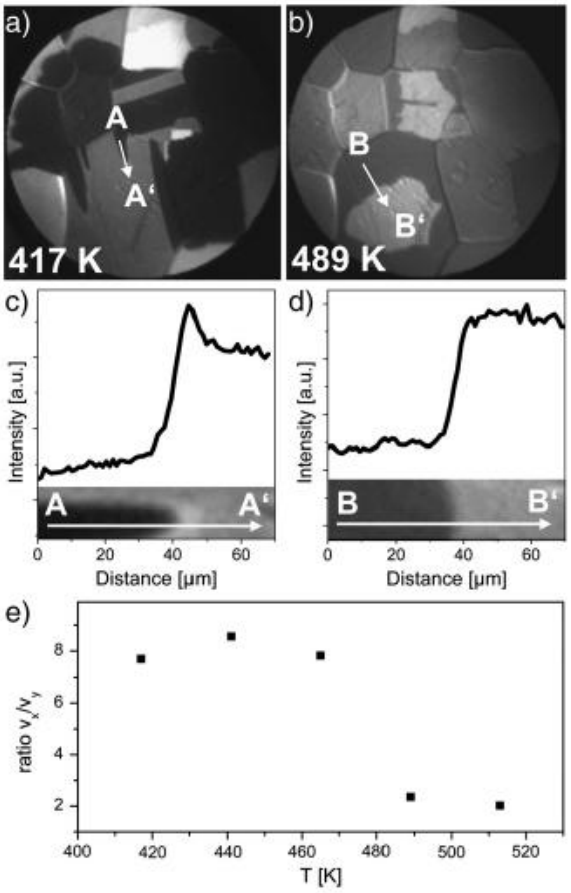

Fig. 6. Oxygen front propagation at two different temperatures of 417 K and 489 K.(a) and (b) PEEM images of oxygen fronts during the transition τ_B at $p_{O2} = 1.3x10^{-5}$ mbar, at 417 K and 513 K, respectively .(c) and (d) Corresponding intensity line scans across the oxygen front along AA' and BB'. The bright fringe between the CO- and oxygen-covered regions disappears at the higher temperature. (e) Temperature dependence of the ratio of the propagation velocities along (v_x) and across (v_y) the prolonged grooves on the (100) facet. The anisotropy decreases with increasing surface temperature.

towards the (preadsorbed) oxygen. The bright fringe at the border of the CO fronts was assigned to the clean hexagonally reconstructed surface. This mechanism is still in agreement with the current results on Pt foil.

Next, we consider the behaviour of the oxygen fronts. Figure 6 shows the behaviour of the oxygen fronts propagating during the transition τ_B at different temperatures. At low temperature the oxygen fronts are highly anisotropic, similar to the CO fronts (Fig. 6a). However, with increasing temperature the fronts become almost completely isotropic (Fig. 6b), in strong contrast to the CO fronts, where the anisotropy is maintained at high temperature. Also the appearance of the CO_{ad}/O_{ad} border in the oxygen fronts differs significantly from that of the CO fronts (Fig. 6c, d): for low temperatures (e.g. 417 K), the oxygen front exhibits a very bright fringe between the oxygen- and CO-covered regions. In contrast, at 489 K the fringe has vanished, indicating a different front structure at high temperature. A plot of the ratio of the v_x/v_y, where v_x is the velocity along the grooves and v_y across them (Fig. 6e), demonstrates this convincingly: this ratio decreases from a factor of approximately 8 at 417 K to a factor smaller than 2 at 513 K.

Both the disappearance of the front anisotropy and of the bright fringes indicate a change in the propagation mechanism for oxygen fronts upon increasing the temperature. The oxygen front propagation mechanism (again for oscillatory reaction conditions) has been described in the following way [20]: On the CO-covered surface, which is in the (1x1) phase, oxygen can nucleate at its excess in the gas phase at surface defects. Since the oxygen pressure is roughly 10 times higher than the CO pressure, oxygen adsorption in this region prevails over CO diffusion, so the

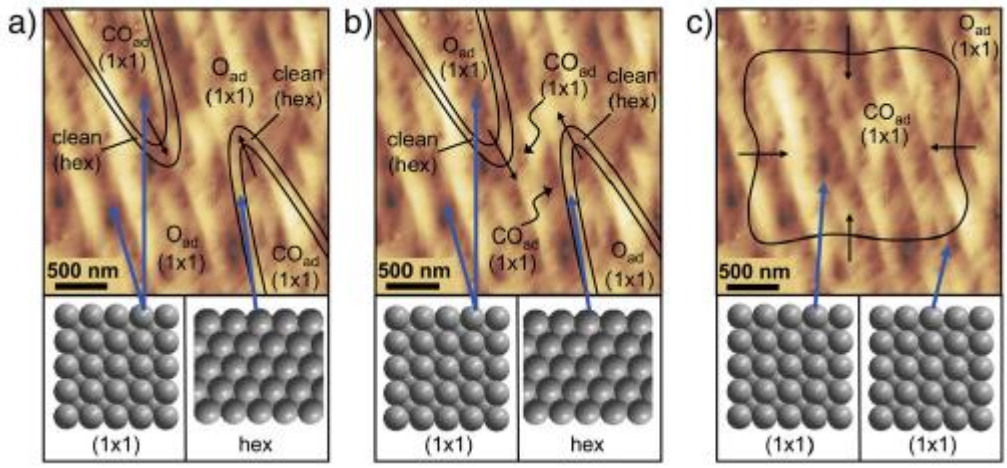

Fig. 7. Scheme of the front propagation mechanism for:(a) CO fronts at all studied temperatures,(b) oxygen fronts at temperatures up to 465 K, (c) oxygen fronts at temperature above 465 K. The AFM image shown in Fig. 4 is used as a background.

oxygen front propagates via the subsequent adsorption of oxygen onto free sites and the (1x1) structure is continuously present across the front line. This mechanism can, in principle, be applied to our high temperature case (489 K – 513 K). It is clear that for a continuous (1x1) structure across the propagating front, no bright fringe should be observed, as also observed in our experiments.

At lower temperatures, we observe a front structure different from that proposed in [20]. Here, the much lower CO diffusion rate leads to a broader front zone than at higher temperature. In this front zone a stronger CO coverage gradient exists and the overlap of the CO_{ad} and O_{ad} coverages is not sufficient to keep the (1x1) structure "stable", thus a nearly adsorbate-free area exists between the oxygen and CO covered regions (therefore a bright fringe is observed, Fig. 6c) which reconstructs to the (hex) phase. The reconstruction is thermally activated starting at temperatures above 390 K [35] and is thus expected to occur under the experimental conditions in Fig. 6c. Interestingly, a similar fringe formation for oxygen fronts was observed earlier [20], but the formation of the (hex) phase within the boundary was excluded as reason, maybe because the fringe-free fronts at which the hex-phase disappears were not observed in Ref. [20].

To finally explain the high anisotropy of the CO-fronts (and the oxygen fronts at temperatures up to 465 K) we refer to the results of the STM study by Borg et al. [36]: the growth of the (1x1) phase is highly anisotropic, thus it is clear that the CO and the oxygen islands, both nucleating the (1x1) structure on the (hex) phase, grow in an anisotropic way as was directly observed in [36] in adsorption experiments. Thus the fronts which propagate in this case via anisotropic island formation, are also anisotropic as well as is schematically depicted in Fig. 7a and b. In turn, on the already existing continuous (1x1) phase the propagation of the reaction front is driven mainly by adsorption which is an isotropic process, thus the anisotropy vanishes for oxygen fronts at T > 465 K, as is observed in the present experiments and is sketched in Fig. 7c.

Last but not least, we mention the role of the reaction-induced mesoscopic "hill and valley" morphology on the surface: it seems that it rather plays a minor role in the observed anisotropy of the reaction front propagation, apart of an apparent effect of the projection of the 3D folded surface to a 2D image in which a circle appears as an ellipse. Our estimations based on the 3D geometry deduced from AFM indicate just a 0.5% contribution to the anisotropy. However, a higher density of steps may be expected across the grooves leading to a certain CO diffusion asymmetry, the contribution of which can be hardly estimated at present.

4. Summary

The domain-specific kinetics of the CO oxidation reaction on individual [100]-oriented domains on a polycrystalline Pt foil was examined by PEEM. The kinetic phase diagram for CO oxidation on a single Pt(100) domain was obtained by intensity analysis of *in situ* video-PEEM images. Such a local kinetic phase diagram provides information within the parameter space (p_{CO}, p_{O2}, T) for regions of high and low reactivity and the bistability region, for a μm-sized Pt(100) surface confined by grain boundaries. The local (PEEM-determined) kinetic phase diagram for Pt(100) domains differs significantly from the averaged (MS-measured) diagram for the entire polycrystalline sample, stressing the necessity of local kinetic studies on heterogeneous samples.

PEEM monitoring of the reaction front propagation on Pt(100) domains reveals a high degree of propagation anisotropy both for oxygen and CO fronts (on the

apparently isotropic Pt(100) surface). The anisotropy vanishes for oxygen fronts at temperatures above 465 K, but remains for CO fronts at all temperatures studied, in the range of 417 to 513 K. A change in the front propagation mechanism is proposed to explain the observed effects.

In turn, the reaction-induced mesoscopic "hill and valley" morphology on the surface, observed by AFM, seems to play rather a minor role in the observed anisotropy of the reaction front propagation.

Acknowledgements

Technical support by Johannes Frank (IMC, TU Vienna) is cordially acknowledged. This work was partially supported by FWF Austria (SFB-F45-04 FOXSI) and by ÖAD, Project 77ÖU14.

References

1. G. Ertl, Angew. Chem. Int. Ed. 47 (2008) 3524-3535 (Nobel Prize lecture) and references therein.
2. V.P. Zhdanov and B. Kasemo, Surf. Sci. Rep. 20 (1994) 113-189.
3. Y. Suchorski, J. Beben, and R. Imbihl, Prog. Surf. Sci. 59 (1998) 343-354.
4. Y. Suchorski, J. Beben, E.W. James, J.W. Evans, and R. Imbihl, Phys. Rev. Lett. 82 (1999) 1907-1910.
5. Y. Suchorski, C. Spiel, D. Vogel, W. Drachsel, R. Schlögl, and G. Rupprechter, ChemPhysChem 11 (2010) 3231-3235.
6. G. Ertl, Science 254 (1991) 1750-1755.
7. G. Ertl, P.R. Norton, and J. Rüstig, Phys. Rev. Lett. 49 (1982) 177-180.
8. M.P. Cox, G. Ertl, R. Imbihl, and J. Rüstig, Surf. Sci. 134 (1983) L517-L523.
9. R.J. Behm, P.A. Thiel, P.R. Norton, and G. Ertl, J. Chem. Phys. 78 (1983) 7437-7447.
10. P.A. Thiel, R.J. Behm, P.R. Norton, and G. Ertl, J. Chem. Phys. 78 (1983) 7448-7458.
11. K. Griffiths, T.E. Jackman, J.A. Davies, and P.R. Norton, Surf. Sci. 138 (1984) 113-124.
12. P.R. Norton, K. Griffiths, and P.E. Bindner, Surf. Sci. 138 (1984) 125-147.
13. R. Imbihl, M.P. Cox, G. Ertl, H. Müller, and W. Brenig, J. Chem. Phys. 83 (1985) 1578-1587.
14. M. Ehsasi, M. Berdau, T. Rebitzki, K.-P. Charle, K. Christmann, and J.H. Block, J. Chem. Phys. 98 (1993) 9177-9184.
15. M. Berdau, A. Karpowicz, G.G. Yelenin, K. Christmann, and J.H. Block, J. Chem. Phys. 106 (1997) 4291-4308.
16. Y. Suchorski, R. Imbihl, and V.K. Medvedev, Surf. Sci. 401 (1998) 392-399.
17. H.H. Rotermund, S. Jakubith, A. von Oertzen, and G. Ertl, J. Chem. Phys. 91 (1989) 4942-4948.
18. A. von Oertzen, H.H. Rotermund, S. Jakubith, and G. Ertl, Ultramicroscopy 36 (1991) 107-116.
19. H.H. Rotermund, W. Engel, M. Kordesch, and G. Ertl, Nature 343 (1990) 355-357.
20. J. Lauterbach and H.H. Rotermund, Surf. Sci. 311 (1994) 231-246.
21. B. Rausenberger, W. Swiech, W. Engel, A. Bradshaw, and E. Zeitler, Surf. Sci. 287/288 (1993) 235-240.
22. B. Rausenberger, W. Swiech, C.S. Rastomjee, M. Mundschau, W. Engel, E. Zeitler, and A.M. Bradshaw, Chem. Phys. Lett. 215 (1993) 109-113.
23. W. Swiech, B. Rausenberger, W. Engel, A.M. Bradshaw, and E. Zeitler, Surf. Sci. 294 (1993) 297-307.
24. W. Swiech, C.S. Rastomjee, R. Imbihl, J. W. Evans, B. Rausenberger, W. Engel, A. K. Schmid, A.M. Bradshaw, and E. Zeitler, Surf. Sci. 307-309 (1994) 138-142.
25. H.H. Rotermund, J. Lauterbach, and G. Haas, Appl. Phys. A 57 (1993) 507-511.
26. J. Lauterbach, K. Asakura, and H.H. Rotermund, Surf. Sci. 313 (1994) 52-63.
27. J. Lauterbach, G. Haas, H.H. Rotermund, and G. Ertl, Surf. Sci. 294 (1993) 116-130.
28. J. Lauterbach and H.H. Rotermund, Catal. Lett. 27 (1994) 27-32.
29. Y. Uchida, G. Lehmpfuhl, and R. Imbihl, Surf. Sci. 234 (1990) 27-36.
30. H. Wei, G. Lilienkamp, and R. Imbihl, Chem. Phys. Lett. 389 (2004) 284-288.
31. C. Spiel, D. Vogel, Y. Suchorski, W. Drachsel, R. Schlögl, and G. Rupprechter, Catal. Lett. 141 (2011) 625-632.
32. F. Schlögl, Z. Phys. 248 (1971) 446-458.
33. F. Schlögl Z. Phys. 253 (1972) 147-161.
34. P. Heilmann, K. Heinz, and K. Müller, Surf. Sci. 83 (1979) 487-497.
35. P.R. Norton, J. Da Vies, D. Creber, C. Sitter, and T. Jackman, Surf. Sci. 108 (1981) 205-224.
36. A. Borg, A.-M. Hilmen, and E. Bergene, Surf. Sci. 306 (1994) 10-20.
37. P. van Beurden, B.S. Bunnik, G.J. Kramer, and A. Borg, Phys. Rev. Lett. 90 (2003) 066106.
38. E. Ritter, R.J. Behm, G. Pötschke, and J. Wintterlin, Surf. Sci. 181 (1987) 403-411.
39. A. von Oertzen, H.H. Rotermund, S. Nettesheim, Surf. Sci. 311 (1994) 322-330.
40. P. van Beurden, and G.J. Kramer, J. Chem. Phys. 121 (2004) 2317-2325.
41. R. Luther, Z. Elektrochem. 12 (1906) 596-600.
42. Y. Suchorski, J. Beben, and R. Imbihl, Ultramicroscopy 73 (1998) 67-72.